Manufacturing Cost Model for Planar 5 kWel SOFC Stacks at Forschungszentrum Jülich

S. Harboe[a], A. Schreiber[b], N. Margaritis[c], L. Blum[d], O. Guillon[a,e], N.H. Menzler[a]

[a] *Institute of Energy and Climate Research, IEK-1, Materials Synthesis and Processing, Forschungszentrum Jülich GmbH*
[b] *Institute of Energy and Climate Research, IEK-STE, Systems Analysis and Technology Evaluation, Forschungszentrum Jülich GmbH*
[c] *Central Institute for Engineering, Electronics and Analytics, ZEA-1, Engineering and Technology, Forschungszentrum Jülich GmbH*
[d] *Institute of Energy and Climate Research, IEK-3, Electrochemical Process Engineering, Forschungszentrum Jülich GmbH*
[e] *JARA Energy, Aachen, Germany*

Abstract

A study is performed on the manufacturing costs of planar Jülich Solid Oxide Fuel Cell (SOFC) stacks, based on anode-supported cells (ASC). The manufacturing of two ASC concepts with different design approaches (referred to as standard and light-weight) are evaluated on the basis of stacks that have undergone performance and degradation testing. A bottom-up cost model for 5 kWel is constructed to estimate the costs at production volumes of 1 MWel, 10 MWel and 25 MWel per annum. The direct costs of manufacturing are estimated as 2737-1210 €kWel^{-1} for the standard design, and 2170-580 €kWel^{-1} for the light-weight design, depending on production volume. For the evaluated concepts, the material costs are estimated to be dominant over the other factors (at the 25 MWel per annum scale >65 %) which is in accordance with most previous studies. The effect of the different design types on the costs is discussed. The steel components are found to be the most cost-intensive, benefiting the light-weight design. Cost sensitivity analyses to manufacturing parameters, power density and degradation are performed, as well as a theoretical scenarios calculated based on low-cost steel type SS441 replacing the costly Crofer materials and co-sintering replacing sequential sintering. The results are compared to previous studies. Strategies for cost-saving are discussed based on 20 years of experience with stack building and testing in Jülich.

Keywords: solid oxide fuel cell stacks manufacturing, manufacturing costs, bottom-up cost analysis

1. Index

Abbreviations

8YSZ	8 mol-% Yttrium Stabilised Zirconia
APS	Atmospheric Plasma Spraying
ASC	Anode-Supported Cell
ASR	Area specific resistance
CAPEX	Capital expenditure
CHP	Combined Heat and Power
CS^V	Anode-supported cell stack from Jülich (light-weight design)
ESC	Electrolyte-Supported Cell
$F^{III}20$	Anode-supported cell stack from Jülich (stationary applications)

FCE	FuelCell Energy, Inc.
GDC	Gadolinium Doped Ceria
IC	Interconnector
ISC	Inert-Supported Cell
LCC10	$LaMn_{0.45}Co_{0.35}Cu_{0.20}O_3$
LSCF	$La_{0.58}Sr_{0.40}Fe_{0.80}Co_{0.20}O_{3-d}$
LSM	$(La_xSr_{1-x})_yMnO_3$
MCF	$Mn_{1.0}Co_{1.9}Fe_{0.1}O_4$
MEA	Membrane electrode assembly
PVD	Physical Vapour Deposition
SOFC	Solid Oxide Fuel Cell
SP	SOLIDPowers, Inc.
VPS	Versa Power Systems, Inc.
WPS	Wet Powder Spraying

2. Introduction

Fuel Cell systems are rising technologies for supplying clean, efficient power over a wide range of applications. SOFCs are ceramic-based systems with solid electrolyte, operating at temperatures between 600-1000 °C. Of all fuel-to-electrical energy conversion systems, fuel cells offer the highest electrical efficiencies. They have high quality heat as by-product, and can operate on various fuel types including: H_2, natural gas [1, 2], and to some degree, syngas [3, 4]. Despite the advantages of SOFCs. its commercialisation has been limited by the relatively high manufacturing costs. Overviews from the year 2017 of commercial SOFC products are available in literature [5, 6]. There are various types of SOFC designs available, where tubular and planar cell geometries are well established. Amongst the planar designs is the anode-supported-cells (ASC) concept. The ASCs are designed so that cell's mechanical support is provided by the anode layer (thus, this is the thickest layer, example given in Figure 1). At the Forschungszentrum Jülich, anode-supported SOFCs and their related stacks and systems have been developed for more than 20 years. Under small scale laboratory conditions, very high performance has been reached, including cells with a maximum current density of 3.75 Acm^{-2} (at 750 °C at 0.7 V with H_2/air) [7]. However, such high performance has not yet been reached within real stacks (but instead around 30 % of this value), which shows the challenge lying within the conceptualisation and optimisation of SOFC stacks. As well, the Jülich ASC are the world-wide record holders of SOFCs life-time performance, having now reached more than 93,000 h of continuous operation (last reported by Blum et al. [8]). The linearly averaged degradation rate of APS coated short stacks is 0.3 $\%(kh)^{-1}$ [8].

In this work a bottom-up cost analysis for the manufacturing of stacks has been set up (for previous studies on SOFC see Table 1). Bottom-up cost analysis refers to that the costs are calculated from each cost element upward, which are then summarized in a total cost-estimate. By identifying the dominant cost-factors with a sensitivity analysis, special focus on the accuracy of these cost-elements should be set. This type of cost-estimate requires a detailed understanding of the stack design and performance as well as production methods. Design specifications and speed of manufacturing and their effects on the stack performance are crucial for realistic estimates. Furthermore, when all elements are assumed to be produced

in-house, the analysis is best suited for larger production volumes, since lower production volumes does not allow high machine utilization.

Learning curves are another faster approach for cost-estimates, as previously reported for SOFC [9]. In this method, the scale-up is done by mathematical interpolation/extrapolation beyond the collected cost data. One limitation of this principle is that reliable cost-data for a large range of production volume must be available. The cost-estimate is only descriptive for one design and does not give insight to the impact of different cost elements, thus possible improvements cannot be evaluated . Furthermore, non-linear effects, such as changes in production techniques and investment with increasing scale, cannot be found by linear extrapolation or interpolation. Due to these limitations, this method was not chosen for the present work.

Studies of manufacturing costs of stacks and/or systems are listed in Table 1. As given in the table, some of these studies are bottom-up cost calculations which give insight to the generation of the costs on a detailed level, based on input from various SOFC vendors [10, 11, 12, 13, 14, 15]. These studies were performed by independent institutions, not by the manufacturers, and were commissioned by the Authorities. Their concepts are to our knowledge generic to some degree, and may not be the exact concepts which have been manufactured and tested. For competitive reasons manufacturers do not generally publish detailed manufacturing data, thus the costs analyses from VPS/FCE [16] and SP [11] are black-box analyses which do not give the exact information how the costs are generated, nor the challenges and successes in achieving cost-benefits. In conclusion, bottom-up cost studies published from stack builders themselves are to our knowledge lacking. Furthermore, the bottom-up cost studies on ASCs [10, 11, 12, 13, 14, 15, 17, 18, 19, 20, 21] are all based on concepts which vary quite significantly from the Jülich designs. Whereas Jülich has focused on maximizing power density and minimize degradation using in some cases more specialized and expensive materials, the previous cost studies are based on concepts in which some of the materials are replaced by low-cost alternatives.

Table 1: Overview of cost targets and literature available with manufacturing cost analyses of stationary SOFC systems (- not available).

Source	**Utilisation**	**Stack design**	**Prod. scale [MW year^{-1}]**	**Max. unit capacity**	**Cost analysis**
DOE target 2020 [22]	stationary CHP	-	-	-	system <1500 US$ kWel^{-1}
Seca program target [23]	power island factory	-	-	-	stack <175 US$ kWel^{-1}
Versa Power Systems [16]	"-"	VPS/FCE (ASC)	570	25 kWel (>100 MWel)	black box
SP [11]	stationary CHP	SP (ASC)	2-50	-	black box
George et al. [24]	stationary	Westinghaus (tubular)	100-450	-	black box
Gardner et al. [25]	stationary	Rolls-Royce (MEA)	100-2000	0.2-20 MWel	black box
Thijssen [10]	"-"	based on FCE/VPS (ASC)	5	-	bottom-up
Scataglini et al. [11, 12]	stationary CHP	based on FCE/VPS (ASC)	0.01-1250	1-250 kWel	bottom-up
Battelle [13]	stationary CHP	generic (ASC)	0.5 -250	1-250 kWel	bottom-up
Weimar et al. [14]	APU	Based on Delphi Gen4 (ASC)	-	259 kWel	bottom-up
James et al. [15]	stationary CHP	based on NexTech Flexcell (ESC)	0.5-2500	5 kWel	bottom-up
Otomo et al. [17]	stationary CHP	generic (ISC)	70	1 kWel	bottom-up
Otomo et al. [18]	stationary CHP	generic (ISC)	22-2200	220 kWel module	bottom-up
Carlson et al. [19]	power island factory	generic (ASC)	10-1000	5 kWel	bottom-up
Ippomatsu et al. [20]	-	Westinghouse-type tubular cells	200-375	-	bottom-up
Soydan et al. [21]	-	ASC micro-tubular	(5-500) $\times 10^{-6}$	-	material and energy cost
This work	stationary CHP	Jülich prototype (ASC)	10-250	5 kWel	bottom-up

In this article, a detailed insight is offered to the ASC cell and stack designs, material demands, as well as proposed manufacturing techniques from Jülich. The study is based on concepts which in order to have gone under long term testing from the years 2010-2013. A bottom-up cost model for 5 kWel stacks is constructed for production volumes of 1, 10 and 25 MWel per year. Sensitivity analysis of the various cost elements, power density and degradation is performed. As well, theoretical scenario calculations for a low-cost steel type, SS441 and co-sintering are performed. Challenges and opportunities in decreasing the various cost factors are discussed, and the results are carefully compared to those of previous cost studies. From the analyses and evaluation, important areas of research and technical development to reduce manufacturing costs of SOFC stacks are suggested.

3. Anode-supported cell stacks

3.1. Jülich anode-supported cell stacks

For the study, two ASC stack concepts from Forschungszentrum Jülich are evaluated: the $F^{III}20$ stack (standard design, developed for stationary applications) [1] and the CS^{V} stack (light-weight design) [26]. Schematics of the component layers, the IC designs and the stacking concept are given in Figure 1. The stacks physical characteristics and operation conditions are given in Table 2. Degradation is evaluated to find the averaged lifetime performances. Degradation behaviour of the stacks can be found in previous reports; $F^{III}20$ [1, 27] and CS^{V} [28]. Technical targets for fuel cell stationary systems Combined Heat and Power (CHP) [22] include operating lifetime of 60,000 h. For the base-case analysis it is assumed that the stacks are able to reach the life-time target and the degradation rate is constant over the lifetime.

Table 2: SOFC stack properties and operation conditions, based on reference stack test.

Stack	**$F^{III}20$**	**CS^{V}**
Footprint [mm^3]	371x224x145	180x205x138
n layers	18	60
Active area per layer [cm^2]	361	128
Weight [kg]	73.5	20.6
Operation conditions		
T [°C]	700	770
fu [%]	70	40
Gas	CH_4 (intern. reform)	H_2:Ar:H_2O=45:45:10
$\dot{V}_{fuel}$ [$lmin^{-1}$]	100	105
$P_{0,el.}$ [W]	2400	1884
Cell area power density [Wcm^{-2}]	0.37	0.245
Volumetric power density [Wl^{-1}]	199	370
ASR at 750 °C and 0.3–0.5 Acm^{-2} [$m\Omega \times cm^2$]	285	345
d_{rate} [$\%kh^{-1}$]	0.3 [1]	0.4
Test duration [h]	5,000 [1]	1,700
$P_{avg,60kh}$ [Wcm^{-1}]	0.35	0.23
n_{stacks} per 5 $kWel_{Avg}$	2.29	3.02

Materials and manufacturing: Overview of the manufacturing processes for the two stack concepts (scaled to 5 kWel with the energy and material net-inputs as found within the present work) are given in Figures 2 and 3. Listed below is information on the manufacturing steps of the ASC stacks:

- Cells: schematics of the respective cell layer thicknesses and their materials (LSCF cathode, GDC barrier layer, 8YSZ electrolyte and 8YSZ/Ni cermet anode and anode support) are given in Figure 1. The only difference between the two cell types is the thicker anode substrate, which may affect

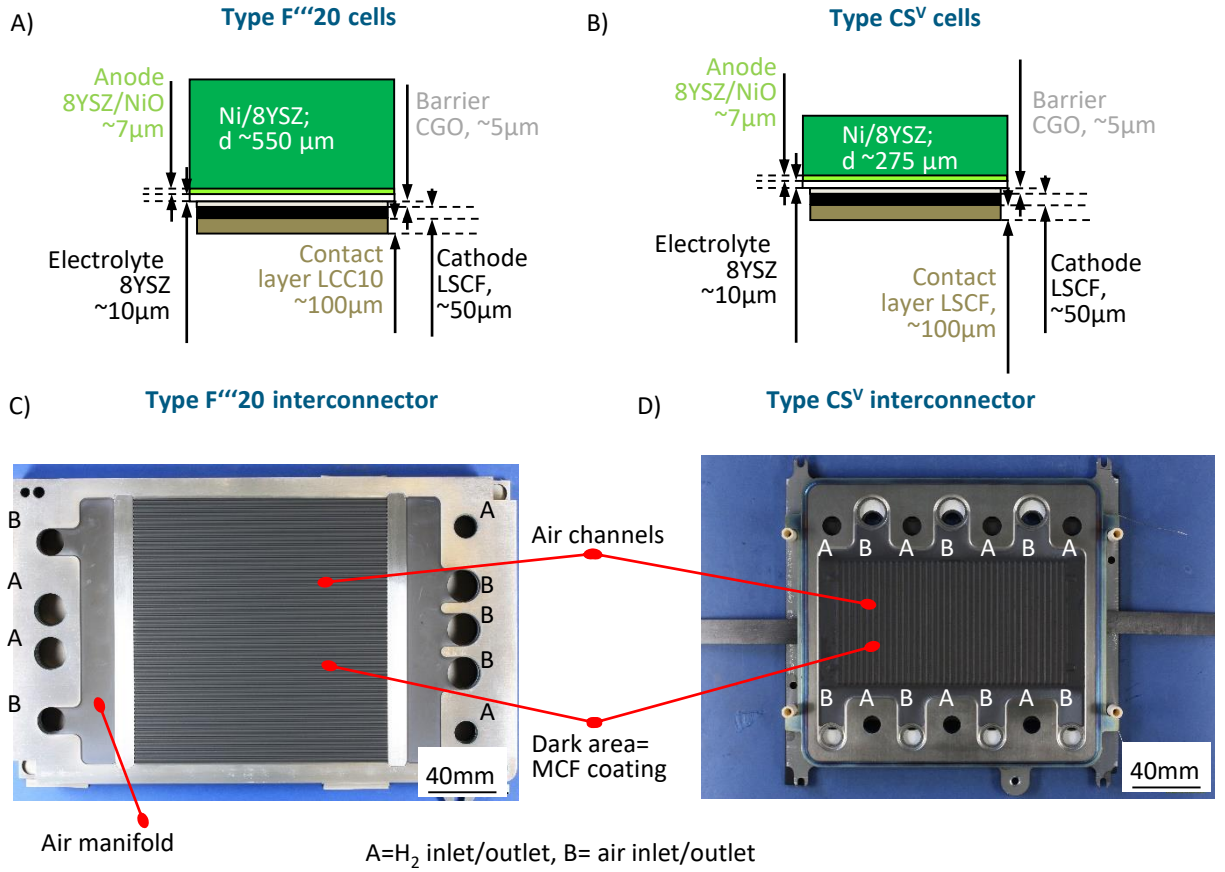

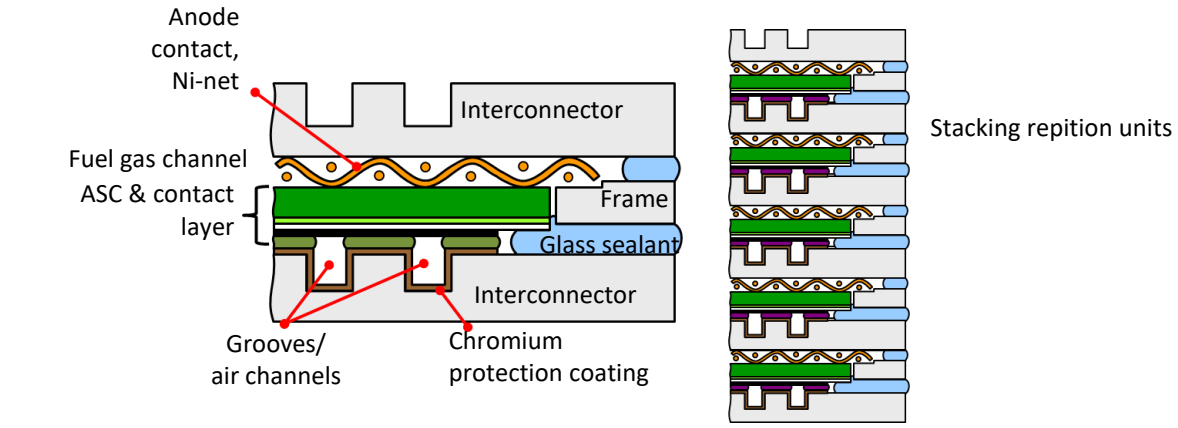

Figure 1: Geometry of ASC cross-section and contact layer thicknesses (drawings not to scale) A) F^{III}20, B) CS^V. Photographs of IC with APS coating (shown from cathode/air side): C) F^{III}20, D) CS^V. E) Stack components and placement of components.

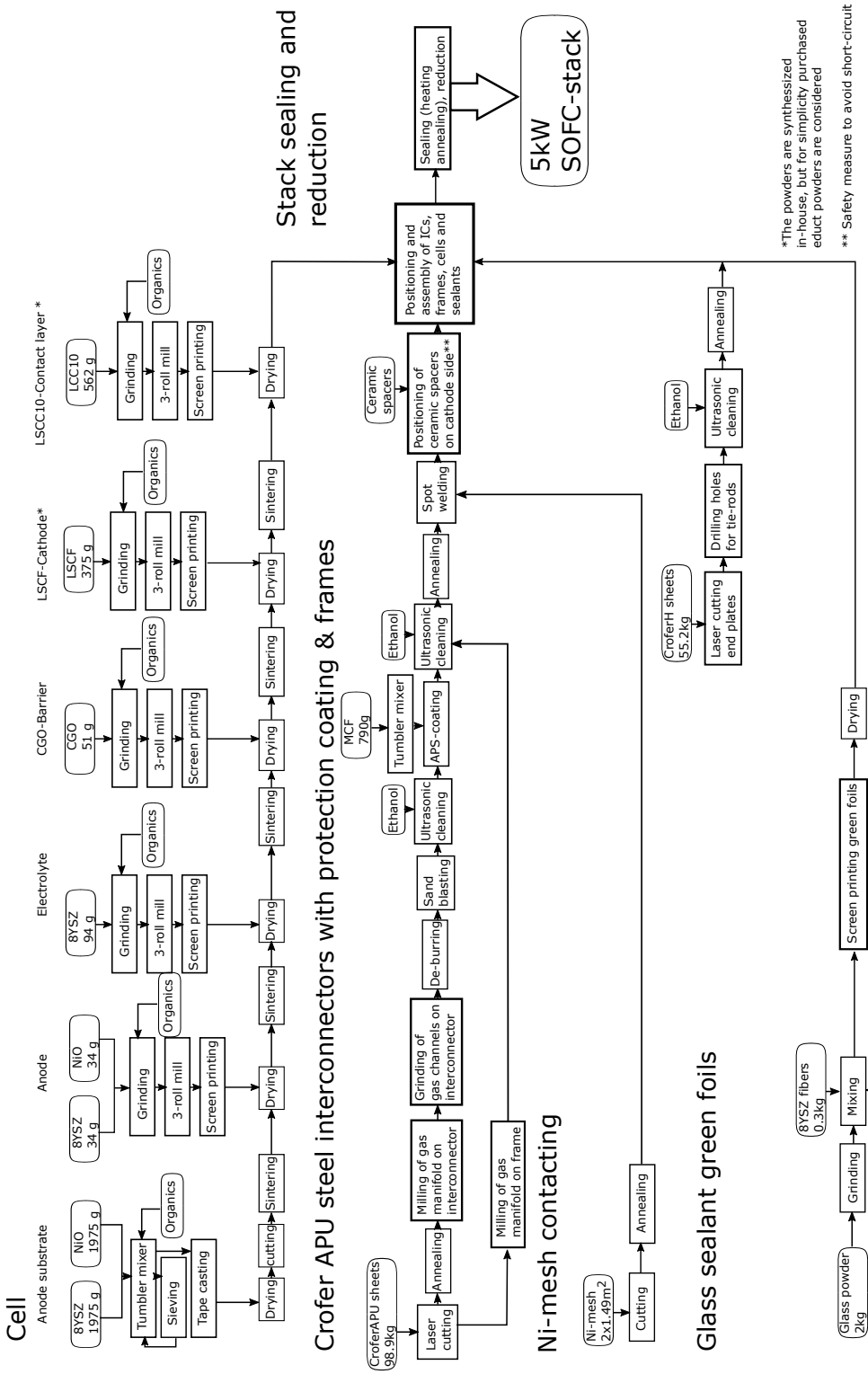

Figure 2: Schematic showing the manufacturing process and the net-material demands during manufacturing, as found within the present work of the $F^{III}20$ stack-concept, scaled to 5 kWel.

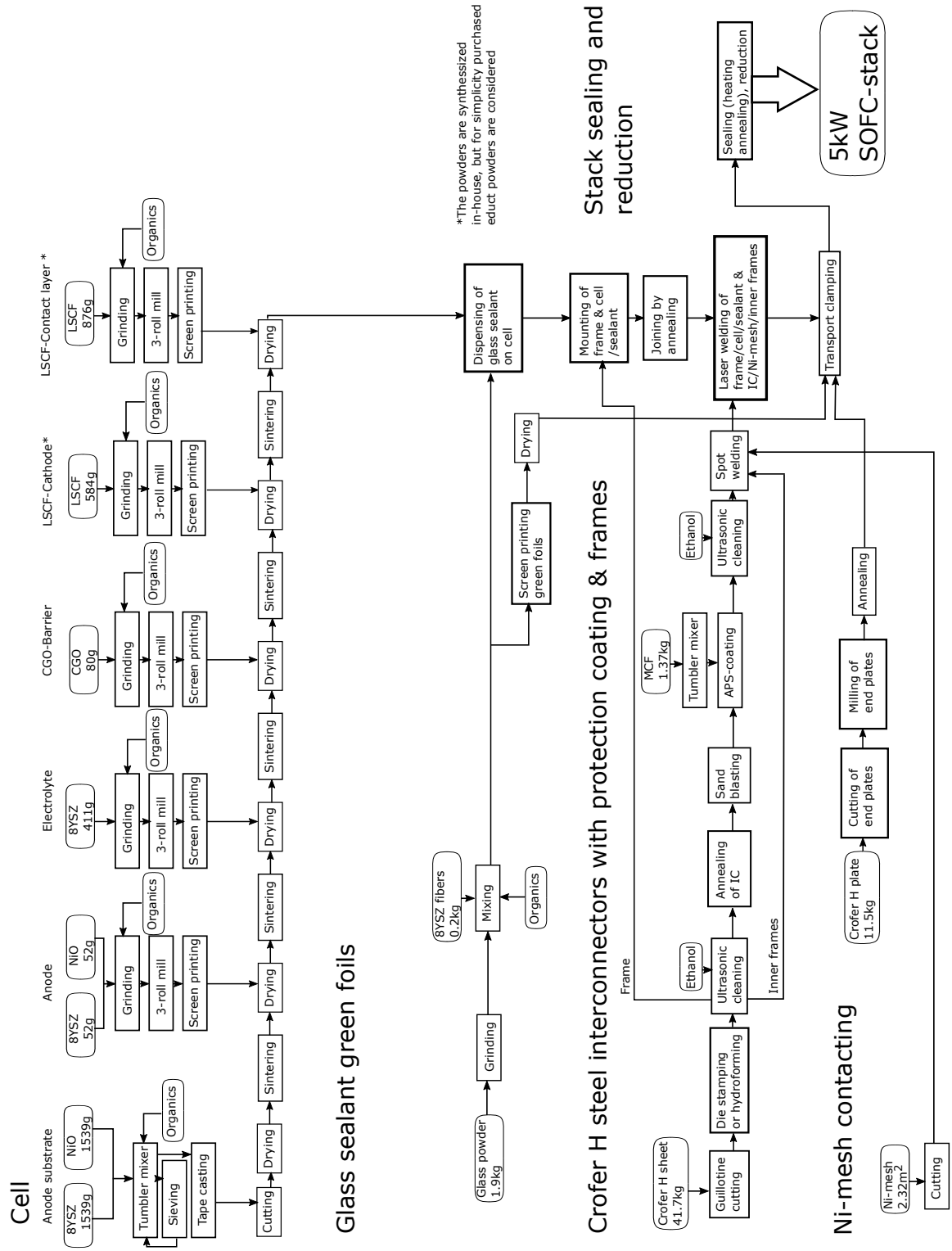

Figure 3: Schematic showing the manufacturing process and the net-material demands during manufacturing, as found within the present work of the CS^V stack-concept, scaled to 5 kWel.

mechanical stability but not electrochemical performance. The contact layers of the cells also differs; LSCF and LCC10 are used interchangeably as a contact layer, their effect on on power density are negligible. Both have been tested in various generation of stacks, to see the effect of perovskite composition on degradation. In the more recent stacks LSCF is used as LCC10 has additional degradation issues [29]. The production route of the cells, involving screen printing and tape casting of the layers, is discussed in [30]. The anode substrate is tape cast and sintered, then the other layers are added by screen printing, dried and sintered one-by-one. For both these cell types a sequential sintering route was applied, meaning that for each layer a sintering step with optimised temperature was used [30].

- Sealant: The glass-cermet used is discussed by Gross et al. [31]. The slurry contains glass powders, 8YSZ fibres and organics. Green foils are made from the slurry by screen printing, which are placed between the joining steel components. The sintering of the glass seal occurs in a separate annealing step before complete stack assembly in the CS^V design, and only in the final step of annealing step of the complete stack in $F^{III}20$.

- Contacting: for the IC material, matching thermo-mechanical properties with the cells is crucial for long-term performance. The Crofer materials were developed for this purpose as well as to have low Cr-evaporation rates to maximise stack lifetime. However the Cr-evaporation rate of the Crofer materials have been found still too high to inhibit Cr-poisoning (very low amounts of Cr is enough to decrease cell performance). Hence, additional Cr-protection coating is necessary for long-term stability. The IC material for stack $F^{III}20$ was developed by Quadakkers and colleagues [32]. In this stack the commercial alloy Crofer22APU is applied. This alloy is vacuum-cast (and therefore of relatively high cost, 25-20 €kg^{-1}) and the metal sheets applied for the IC have a thickness of 2.5 mm in order to be creep and corrosion resistant at operation temperatures [33, 8]. The fuel gas and air manifolds were finished by milling, the air channels are prepared by creep-feed grinding, and the outer line by laser-cutting. These form-shaping steps cause deformation of the steel, so that additional annealing steps are required to flatten the parts. For stack CS^V the development of the IC material is described by Froitzheim et al. [34], and the alloy is commercialised as Crofer22H. Crofer22H has a higher oxidation resistance and creep strength than Crofer 22APU. Thus, thinner sheets can be applied compared to the $F^{III}20$ design. In the design 0.3 mm sheets are applied, these are thin enough to be cold-formed to achieve the shape of the gas channels, and the sheets can be die punched to achieve the outer line. The CS^V has 50 % reduced power density compared to $F^{III}20$. Since the cells are nearly identical, it is reasoned that this is a question of the contacting situation. The specific resistance of the Crofers are comparable: at 700 °C of Crofer22H with MCF APS coating after 1000 h in air was found to be 100-150 mΩcm^{-2} after 1000 h in air [35], that of Crofer22APU at 800 °C with MCF coating after 1000 h in air approximately 96 mΩcm^{-2} [36]. Due to the forming technique of CS^V, the shapes of the IC contacting and gas channels are rounded rather than sharp edged as in $F^{III}20$ which also offers high rigidity (see Figure 1). This leads to smaller contacting areas between the IC and the cell's anode and cathode, respectively, and different contact pressure distribution. The Ni-meshes are different with a thinner thread and larger mesh in the CS^V design, also the distance between the spot welding points is larger. Likely, herewith lies substantial room for improvement, which is currently topic of investigation. The stacks are contacted with Ni-meshes adjacent to the IC on the anode side. In contrast to what has been disclosed for other concepts [12, 11, 13], the nickel mesh for the Jülich ASC concepts is spot-welded to the Crofer plate in order to improve electrical contact. For the $F^{III}20$ stack two Ni-meshes were applied: one for providing gas flow channels with 2 mm mesh size and 0.6 mm wire thickness, and an additional one for spacing between coarse mesh and cell with 0.2 mm mesh size and 0.125 mm wire thickness. In the CS^V one mesh is applied with 2 mm mesh size and 0.3 mm wire thickness.

- Protection coating: the cathode side Cr protection coating material for these stacks is $Mn_{1.0}Co_{1.9}Fe_{0.1}O_4$ (MCF) [37]. The application is performed with the Atmospheric Plasma Spray (APS) process. The coatings achieved with this process are highly dense and have proven excellent durability [37]. Prior to applying the protection coating, the surface is sandblasted and

ultrasonically cleaned in order to obtain the best possible adhesion. An APS-system (Oerlikon Metco, Switzerland) with multi-coat 6-axes robot is used. The thickness of the MCF-coatings in these stacks is 100 µm. The coating is densified during the sealing and operation of the stack. These stacks do not have anode side protection coating. However, previous studies show that after longer operation times also here oxide scales form on the anode side (17,000 h) [38], inter-diffusion of inhibiting elements (30,000 h) [39] and forming of new phases (35,000 h) [40]. It is therefore to debate whether anode side contacting is also required for long-term operation; this would likely lead to increased contact resistance, also since spot welding then cannot be applied.

- After the assembly of the stack, it is annealed at high-temperature with successively Ar and H_2 gasses and air. This serves the purpose of a) sintering of the glass cermet to seal the stack gas-tight and b) reducing the anodic NiO to Ni for an electrochemically active anode.

3.2. Anode-supported cell stacks from previous SOFC cost studies

Comparison is made to previous studies [14, 12, 11, 13]

- Cells and sealants: in previous studies, the cells and sealants were similar to the Jülich types, and manufactured mainly in the same way. Apart from that, most of the studies applied co-sintering [12, 11].
- Contacting: the main differences to the Jülich stacks is that low-cost type of steels were applied for the IC, frames and end-plates. Stainless steels, like SS441, were applied. SS441 is a ferritic stainless steel containing niobium to hinder corrosion and oxidation [41]. The steels were cold formed, for example, by die stamping [14, 12, 11, 13]. Both thickness and widths of the IC and frames were significantly smaller in the previous studies [12, 11, 13, 19] than the Jülich concepts. In the previous report [13], gas channels were not machined in the IC, but instead stainless steel meshes without protection coating were applied on both the cathode and anode sides (Fig. 5-21, 5-24 [13]). This is not realistic, since it is well known that stainless steel would quickly degrade without appropriate coating, leading to a decrease of the conductivity and a mechanical break-down [42]. Tests with the application of a Ni-coated stainless or low carbon steel mesh on the anode side showed limited long-term stability [43]. For the air side, tests are currently ongoing in Jülich on steels coated with cobalt, but to our knowledge no previous studies have shown suitable degradation performance. In previous studies [14, 12, 11, 13], the contacting had not been fixed with spot-welding, it was found in Jülich that welding improves the performance by lowering the contact resistance.
- Protection coating: PVD was applied for the stainless steel VPS/FCE stacks according to the previous study [11]. Another study showed that SS441 coated with APS (with nitride pre-treatment) or PVD exhibited low resistance values after 1000 h of testing in air [35]. PVD reactive sputtering deposition rate is in the range of 0.1-20 nmmin^{-1} [44], and usually just thin layers are applied as protection layers. Thus, the surface roughness of the steel must either be optimized beforehand, or the deposition time must be increased. In previous study PVD coatings of approximately 20 µm were applied [35], which give high cycle times in production. The VPS/FCE stacks have reported for single cell stack P_0 = 0.425 Wcm^{-2} and degradation of 0.36 %(kh)$^{-1}$ for 9000 h [45], and P_0 = 0.34 Wcm^{-2} and degradation of -0.64 %(kh)$^{-1}$ over 4200 h for the 180 W stack [16]. The SP stack with SS441 IC showed 5 µm oxide scales on anode side (no coating) after the 5000 h test, but still low degradation of 0.4 %(kh)$^{-1}$ was reported [42]. Another study showed continuous Mn-Cr oxide scales for thin Ni-wires after the 6000 h test [46].

4. Cost model

The methodology of the model, including the assumption that the production is based on manufacturing taking place in the Western Hemisphere is comparable to previous models [14, 12, 11, 13], it is as follows:

- The number of layers and stacks in order to meet the production target are determined.
- The amount of materials needed is determined for which the costs are calculated.
- The manufacturing flow routes are generated as described in section 3.1. For the manufacturing detailed insight of suitable techniques are well known for lab-scale. Suitable equipment has been chosen partly based on extrapolation of the experience from the prototype manufacturing combined with generally accepted engineering and manufacturing practice, including consultations with external machine shops. The data used has also been calibrated with data from previous studies [12, 11, 13]. There may still be some room for further optimization in the detailed manufacturing methods.
- Machine parks are theoretically constructed to meet the production targets. From this, machining costs are calculated.
- Based on the manufacturing time necessary for the components, the energy demands of the machines are determined, from which the energy costs are calculated.
- From the calculated manufacturing time of the components the labour requirements are determined, from which labour costs are calculated.

The direct cost, C_{tot}, is calculated as

$$C_{tot} = C_{mach} + C_l + C_e + C_{mat} \tag{1}$$

where C_{mach} is the cost of the machinery, C_l is the labour cost, C_e is the energy cost and C_{mat} is the material cost. Cost of buildings have been left out of these calculations as it was found to give near negligible contribution in previous studies [11, 47]. In Table 3, assumptions for the base-case calculations are given.

Table 3: Baseline assumptions for cost model calculations.

Factor	**Value**
Energy cost	0.17 €kWh^{-1} [48]
Currency conversion	0.85 € US$ $^{-1}$
Personnel-hours per year and shift at 7.5 hours net per day	1,800 h

4.1. Material costs

Material net demands are given in Figure 4 A) and B). The net material demands for the cell layers are determined from their geometries, microstructure and weight loss by reduction. The exact calculations and values can be found in supplementary information. The anode substrate is tape cast and laser cut in green form which means that cuts can be recycled into the slurry. In the screen printing process no cuts are generated. This means that the scrap rate for cells raw materials is near negligible. However, the cell manufacturing is sensitive, since small variations in process parameters can lead to microstructural defects such as micro- or even macro cracks making the cells unusable. On lab-scale, yield is not expected to be above 80 %. Assuming that this can be improved by automated procedures, yield factors are set to 85 %, 88 % and 94 % from low to high production scale. Previous study assumed 13 % cell scraps including failed parts at all production scales [13].

For the IC, frames and end plates, the scrap rates are estimated based on the weight of metal sheets minus the weights of the parts, where possible sheet-sizes were discussed with the vendor. The following average values for the stacks are found: F2018-07: 22.4 %, CS^V: 24.3 %. The values appear low due to high relative weight of end plates. Previous study used 20 % for IC's and 72 % for frames [11], which are almost the same values as found here. Other study assumed 10-13 % for IC, and 0 % for frame, where die stamp

operation is applied [13]; these values appear unrealistically low. However, it is claimed that the values in the present study may be decreased by further optimizing the shape of the designs, where scraps are used for other parts. It is assumed that the scraps can be sold for 40 % of the purchase price as done in the previous study [11]. Yield factors are set to 85 %, 88 % and 94 % from low to high production scale, found by interpolation from previous study [11]. The coating net material amount is found by weighing the IC before and after coating. The APS process sprays the slurry on the surface and a relatively large fraction is deposited outside the target. However, by designing a suitable collecting and recycling management of the slurry, the scrap rate is assumed to be near negligible. The glass sealant is produced by screen printing and drying, which do not generate cuts, thus negligible scrap is assumed. The yield is also assumed to be close to 100 %. Previous study assumed scrap of 0 % and yield of 99.5 % [11]. The Ni-mesh is cut in squares, as the manufacturers can provide relatively large widths, thus low scrap rate of 5 % is expected.

Material price data is collected from literature and public vendors. An overview of costs of cell materials is given in Figure 4 C). Despite of discrepancies, a trend in the price differences between the various "classes" of cell materials is clear. It is assumed that LCC10 follows the same price trend as the other perovskite cathode materials LSCF/LSM. The price of the applied Ni-mesh materials is given in Table 4, and that of glass sealant and IC materials are given in Figure 4 D). For the various materials in Figures 4 C) and D) and Table 4, the prices for the requested amounts are estimated from least mean square fits in the form ax^b through the collected data. The price of coating materials is estimated based on the price previously given [11], as 250 €kg^{-1}. It is assumed that materials will be purchased two times per year. Storage cost is assumed to be 5 % of the purchase cost per year.

Table 4: Prices of Ni-meshes (2018) [€m^{-2}], public vendor asked not to be disclosed.

Amount, [m^2]	50	1700	7500
Ni, mesh/wire [mm]			
2/0.6	164	78	75
0.2/0.125	-	48	44
2/0.3	-	29	27

4.2. Machining cost

The costs of machinery per annual production is determined based on a 10 year linear depreciation of the CAPEX value (the CAPEX value refers to purchase and installation cost of machinery excluding tools with high wear such as dies). In addition, 10 % of CAPEX per year for service of the machine is included. Die-costs and creep-feed grinder discs were separately calculated, see supplementary information. Other tool costs and consumables were included within the percentage-addition to the annual machine costs. The CAPEX for the machines have been based on the following main sources: tape casting machines [12], screen printing lines, kilns, annealing furnaces, assembly and testing [11], tumblers and mixers [13]. For Jülich specialised techniques price figures are based on interviewing specialists in the field. For the less expensive and generic machines, consulting machine shops and internet research gave the applied figures.

Availability factor are for all machines assumed to be 80 % for the low volume and 85 % for the higher volumes, taken from interpolation using data from previous study [12]. Another report has provided input on handling times, die-press operations, and laser welding of thin plates [13]. Cycle times for tape casting, screen printing, annealing, sintering, pre-assembly and assembly are based on previous studies [12, 11]. For the processes which are highly specialised for the SOFC stacks of Jülich, the cycle times are determined based on lab process expertise, knowledge from the machine shop, and scaling the data from prototype development to industrial manufacturing. For instance, during the sintering, the steps are given in [30]; for these cells the sequential sintering program was applied, the total sintering time is 67 h. The milling and creep-feed grinding of the Crofer22APU IC in the F^{III}20 design are highly dependent on a careful balance between selection of tool design and the setting of machining parameters to meet industrial mass production requirements. The cycle times are determined by consulting vendors, supplying them with material test

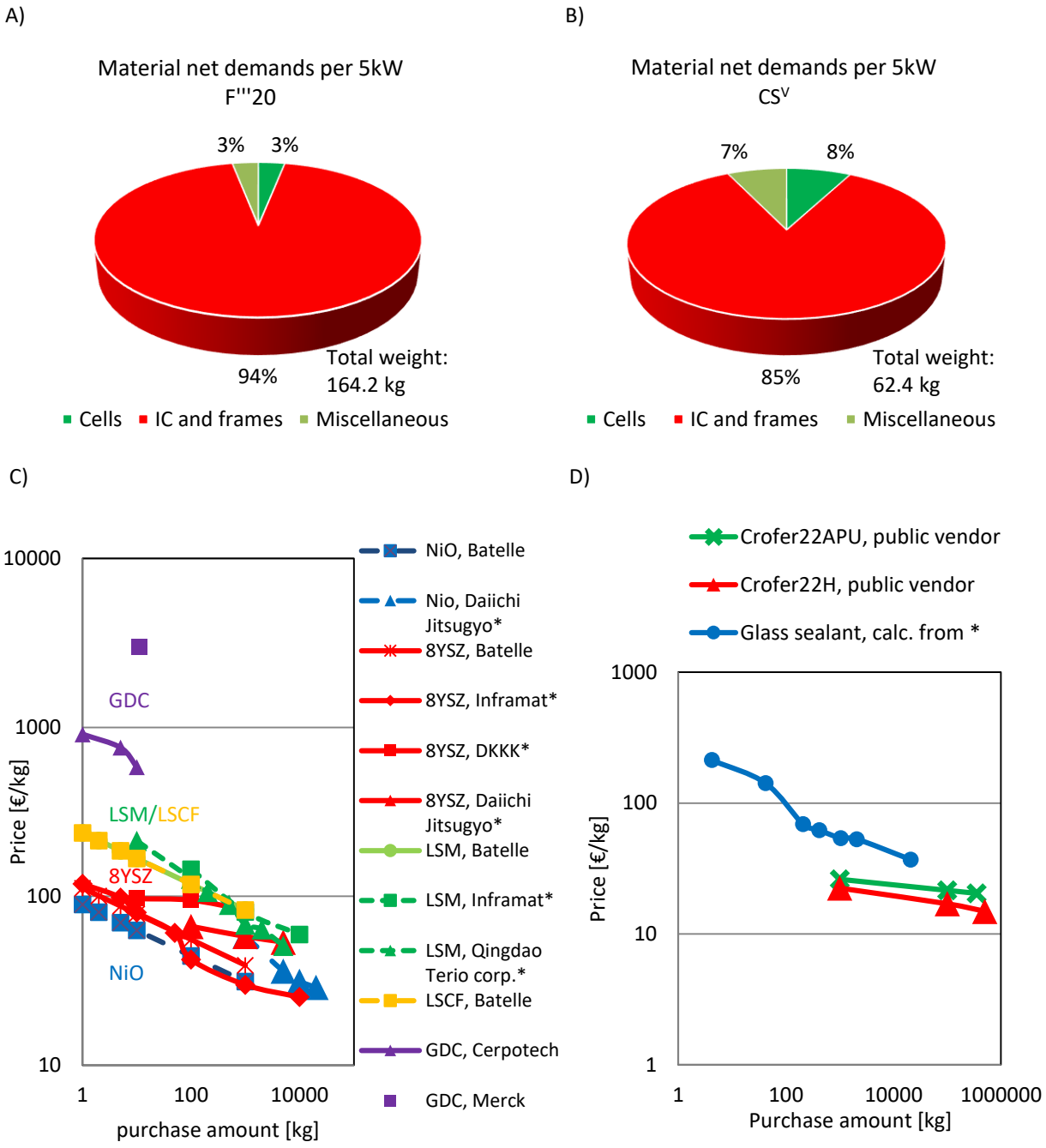

Figure 4: Net material demands per 5 kWel stacks for: A) $F^{III}20$, B) CS^{V}. C) Cell materials from public vendors (2018, where not given otherwise), D) Prices of Crofer sheets (2018, public vendors asked not to be disclosed) and sealant materials over purchase amounts. Those marked with *: [12].

samples from which they then estimated the achievable cycle times. By determining the cycle times values of the manufacturing steps, the necessary equipments are identified. The CAPEX values for the necessary equipments are given in supplementaries.

4.3. Energy costs

The energy consumption for each manufacturing step is determined based on the average power of the machine, as given by the vendor information, and the utilisation time of the machine (see supplementary information). These are based on the power rating of the machines and not accurate values reflecting the variations in power requirement.

4.4. Labour costs

To reflect an expected above average skill level, a somewhat higher element of shift work, and the general salary increase due to a tight labour market, the average hourly cost used for the analyses herein is 40 €. Personnel requirements are decided individually for each operation and scale-dependently (overviews given in supplementary information). For the low level manufacturing it is considered that a large fraction of the labour is done manually and that one person per machine is required. For the medium and high levels production automation robots are included. Automation robots or purpose designed handling devices are commonly used. Previous studies assumed no staff required for automated processes [12, 11], herein a minimum of 0.2 persons have been assumed necessary per machine. Some previous studies assumed lower labour costs and requirements [12, 11, 13], other study assumed a higher labour rate [14].

4.5. Sensitivity analysis

Determination of bounds: the applied materials are specialised and without broad manufacturing competition; hence presuming that manufacturers are reluctant to give out values close to lower price limits, the sensitivity bounds are thus set to -20 % and +10 % of base-case. Bounds for machining costs are based on Monte Carlo simulations for the various cost groups performed with Argo Software [49]. Market evaluation values for minimum, mode, and maximum cost values are applied in the simulations, assuming triangular distributions. From the calculated cost probability distributions of the various cost groups, confidential intervals of 90 % are used to determine lower and upper bounds. Based on evaluation of labour rates abroad to that in Germany the bounds are set to -35 % and +20 %. Electricity prices are assumed to fluctate within bounds of ±20 %.

5. Results and discussion

5.1. Base-case analysis

5.1.1. Direct manufacturing cost per kWel

Figure 5 A) shows the estimated direct manufacturing cost of the stacks and the distribution of the different cost-factors. The cost values and percentages contributed to different cost factors are shown in Table 5 (comparison to previous studies discussed in section 5.5). The CS^V has lower cost, mainly due to the lower material costs. At the 10 $MWely^{-1}$ and 25 $MWely^{-1}$ scales, the materials are the dominant factor in the overall costs of all the stack designs. In Figure 5 B), the distributions of material costs are shown; in $F^{III}20$ steel materials are dominant, in CS^V the distribution is more even between the cost groups, showing that material costs have been lowered in the CS^V, mainly by lowering the costs of steels.

5.1.2. Comparison of stack power densities

CS^V is more cost-effective even though $F^{III}20$ has higher area specific power density. Comparing the Jülich designs based on their materials and manufacturing (see section 3.1), it can be concluded that the cells, protection coating and sealing are nearly identical in these two Jülich stacks, and the lower performance is a question of the contacting situation. In conclusion, the power density of CS^V may be improved mainly by an improved shape design of the air channels (main losses are found on the cathode/air side), and also better Ni contact on the anode side (i.e. finer mesh, higher number of spot welding points), as well as stiffer construction with higher contact pressure.

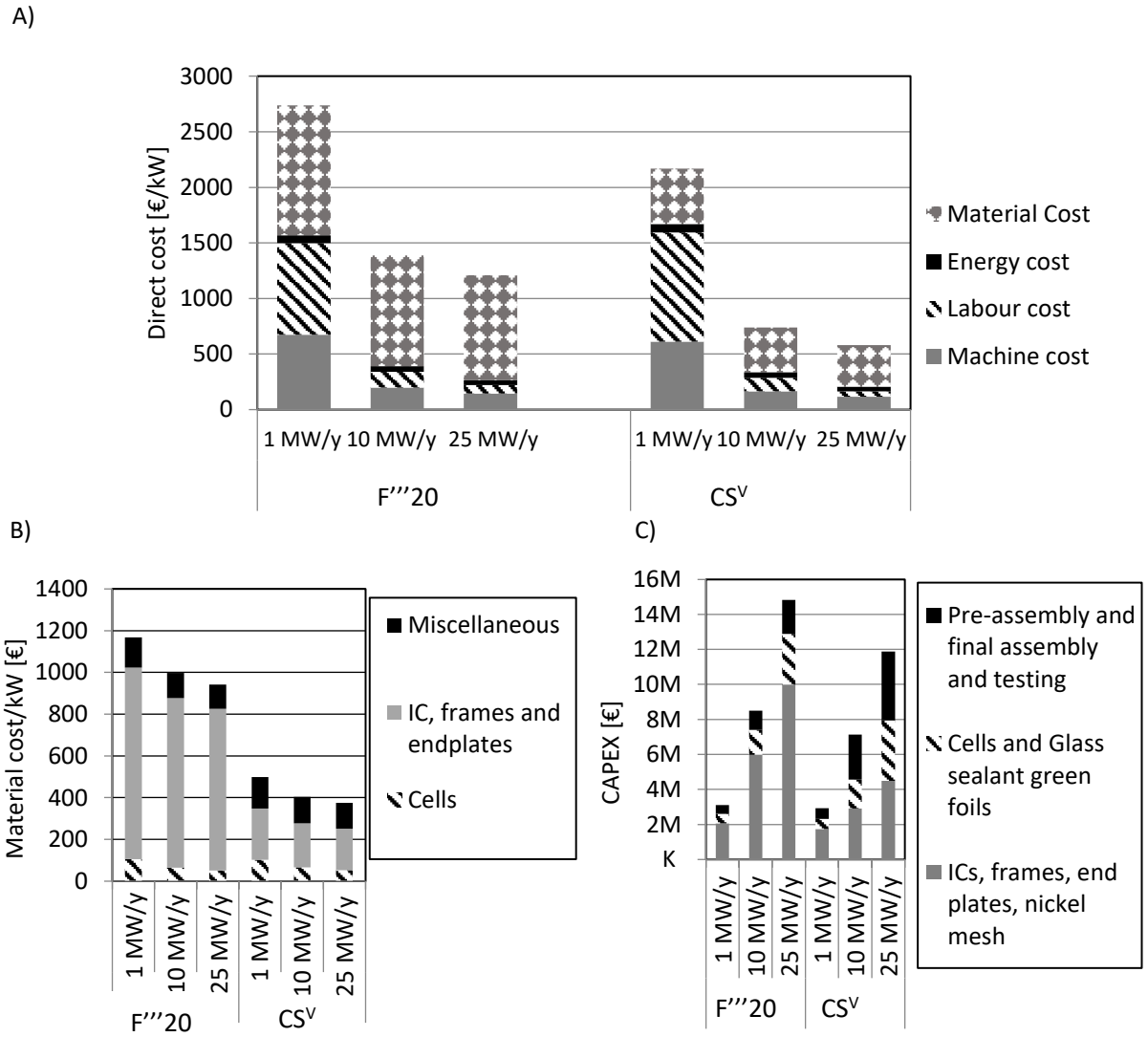

Figure 5: A) Direct costs of the SOFC stack designs at various production volumes, B) costs of materials of the SOFC stack designs at various production volumes, C) CAPEX costs of the SOFC stack designs at the various production volumes.

Table 5: Results of base-case direct manufacturing cost, and comparison to previous studies

	$F^{III}20$	CS^V	Previous studies
Total cost [€kW^{-1}] 1 MWy^{-1}	2737	2170	Given in US$kWel^{-1}:
10 MWy^{-1}	1388	740	90 (5 kWel) [19]
25 MWy^{-1}	1210	580	350 (1000×10 kWel) [11]
			502 (10,000×5 kWel) [13]
Fraction of costs: materials (25 MWy^{-1})	78 %	65 %	Given for high scale prod.: 77 % [16], 81-93 % [47], 35-70 % [11], 55 % [14]
Fraction of costs: labour (25 MWy^{-1})	6 %	9 %	5 % [16], 2-9 % [47], 8 % [11]
Fraction of costs: other (25 MWy^{-1})	16 %	26 %	18 % [16], 25 % [11], 6-10 % [47]
Fraction of costs within material costs (25 MWy^{-1})	$F^{III}20$	CS^V	Previous studies
Steel	82 %	53 %	11-15 % (component level) [12, 11]
Cells	5 %	14 %	50 % (component level) [12, 11]
Miscellaneous	13 %	33 %	35-39 % (component level) [12, 11]
Ni-mesh (part of misc.)	4 %	% 4	

5.1.3. Capital expenditure (CAPEX)

The CAPEX costs are given in Figure 5 C) (more details found in supplementary information). Whereas machinery for IC, frames, end plates, and nickel mesh dominate the costs for $F^{III}20$, for the CS^V design the distribution is more even between the various cost groups. A common theme for the designs is the high investment needed in kilns and furnaces. These are expensive equipments, with estimated costs ranging up to more than 2M € on the 25 MWely^{-1} manufacturing scale. For $F^{III}20$ 2.5 mm Crofer22APU plates, cold-forming techniques are not applicable, therefore, the forming techniques creep-feed grinding and milling have been chosen. These are found to be major production bottlenecks resulting in substantial contributions to the investment costs; estimates reaching up to 4.8M € for the creep-feed grinding and more than 2M € for the milling on the 25 MWely^{-1} manufacturing scale. For the CS^Vstack, this cost is lowered using cold forming techniques. For CS^V, due to the highest number of parts out of the two designs, the assembly process needs the most assembly stations. This leads to an estimated assembly investment costs of nearly 4M € on the 25 MWely^{-1} manufacturing scale. This can be decreased by lowering the number of parts, which has been done in newer versions of the design. APS coating was applied in both ASC concepts. This process has relatively high investment costs, estimated reaching to more than 1.7M € for CS^V on the 25 MWely^{-1} manufacturing scale. Nevertheless compared to some of the other manufacturing steps, APS is not found to be a main bottle-neck. Spot-welding is found to be negligible with investment cost up to 95k € on the 25 MWely^{-1} manufacturing scale.

5.2. Sensitivity analysis

Table 6: Degradation impact on average power density, compared to base-case.

$F^{III}20$ degradation	Average power density 60kh compared to base-case
0.00+%	+9 %
0.25 %	+2 %
0.30 % (base-case)	0 %
0.40 %	-3 %
0.50 %	-6 %
0.75 %	-14 %
1.00 %	-21 %
CS^V degradation	Average power density 60kh compared to base-case
0.00 %	+12 %
0.25 %	+5 %
0.30 %	+3 %
0.40 % (base-case)	0 %
0.50 %	-3 %
0.64 %	-7 %
0.75 %	-11 %
1.00 %	-18 %

In Figure 6 A)-B), the sensitivities of the cost to price uncertainties at 25 MWy^{-1} are given. The sensitivity is highest for the materials; in the $F^{III}20$ design mainly to Crofer steel, and for CS^V towards all material cost groups. For the CAPEX (Figure 6 C)-D), $F^{III}20$ sensitivities are largest towards the manufacturing of the metal parts, and for CS^V towards all manufacturing cost groups. Sensitivity to power density at 25 MWy^{-1} is shown in Figure 6 E). Besides the material costs, the most cost-sensitive parameters is the power density. It is shown for the CS^V that increasing the power density to the values of the $F^{III}20$ (marked goal A), leads to a decrease in the cost of the stack estimated to 378 €$kWel^{-1}$. The effect of degradation rates on the power density (compared to base-case) is given in Table 6, using these values, a significant effect of degradation on the cost can be observed in Figure 6 E).

5.3. Theoretical scenario replacing Crofer with SS441 stainless steel

Due to the high sensitivity to steel costs (section 5.2) a theoretical scenario is calculated, replacing the Crofer steel by the low-cost type SS441. The SS441 steel is used as theoretical scenario calculation for the bottom-up cost models [12, 11, 13]. The material price of SS441 is assumed 1.7€kg^{-1}, estimated from [11]. However, it is well known that stainless steels such as SS441 have a high rate of corrosion at higher temperatures in air atmosphere [42]. Hence, outer surfaces in contact with air must also be coated, in contrast to the Crofers which are stable enough without coating. Areas around air supplies and welds must be thoroughly coated, as corrosion defects can possibly lead to gas leaks. This means the coating surface is increased. In a recent study, SS441 coated with MCF by the APS method (as applied for Crofer) showed low area specific resistance after 1000 h annealing in air (no stack test) [35]. For the present scenario it is assumed that APS can be applied. As a simple approach, double coating material amount and machining effort for coating are assumed. Machining time of the SS441 is also adapted for the $F^{III}20$, since the machining of this alloy is faster. It could be that the application of SS441 changes the power density due to effects such as increased degradation rate, here sufficient stack tests are missing, it is also not conclusive whether SS441 anode side needs coating (see section 3.2). If both IC sides must be coated, spot welding of the Ni mesh to the IC is not possible, which would reduce the power density.

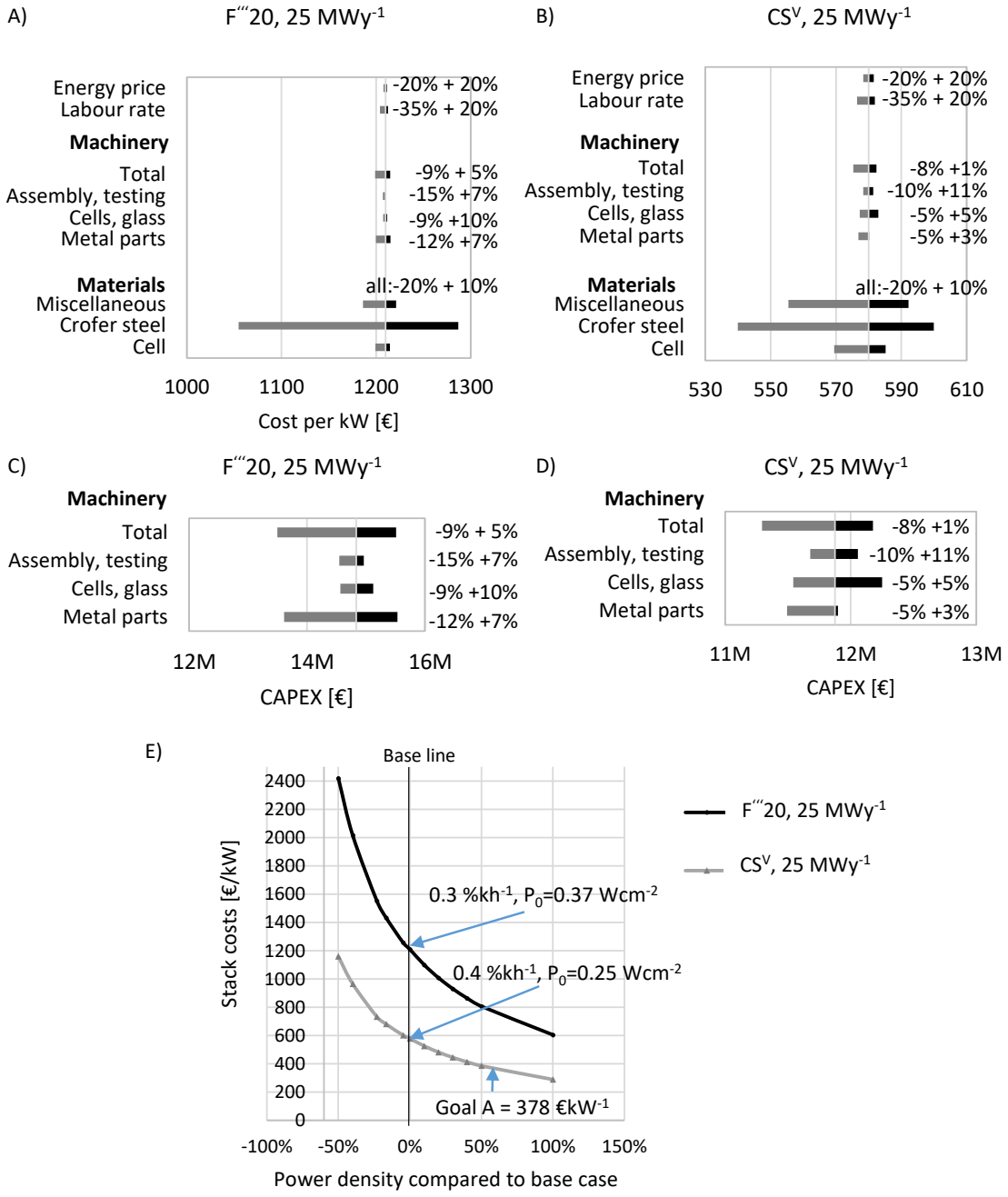

Figure 6: Sensitivity tornado diagrams: A) manufacturing costs per kWel $F^{III}20$ 25 MWy^{-1}, B) manufacturing costs per kWel CS^{V} 25 MWy^{-1}, C) CAPEX $F^{III}20$ 25 MWy^{-1}, D) CAPEX CS^{V} 25 MWy^{-1}, E) Sensitivity to average lifetime power density 25 MWy^{-1}.

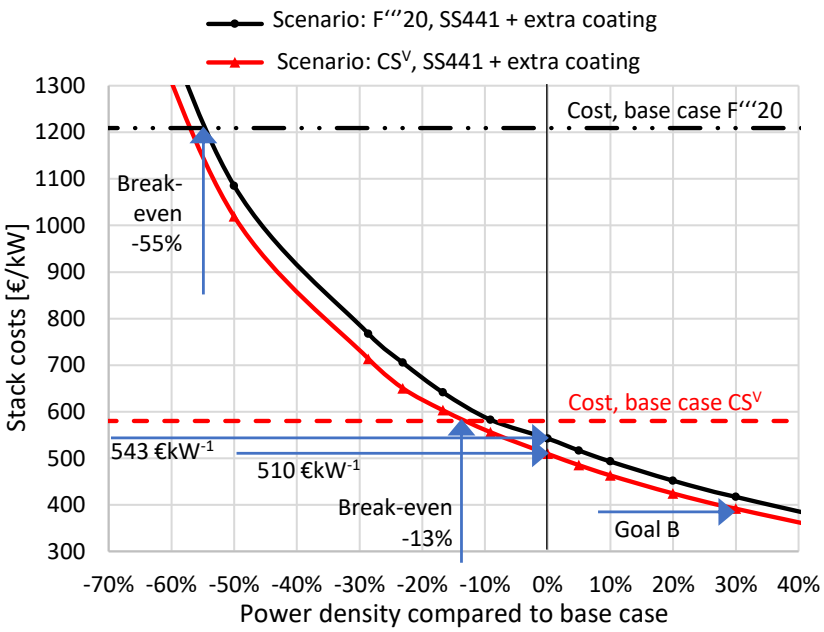

Figure 7: Theoretical calculation scenario applying SS441 steel with adapted machining and coating, estimated stack direct manufacturing cost over cells area power density (0 % corresponds to the area power density of base case).

Thus, in Figure 7 the cost of the scenario with SS441-based design is plotted over power density as a variable. Due to the lower price of SS441, the costs of the stacks decrease. The costs are estimated as 543 €kW^{-1} and 510 €kW^{-1} for F^{III}20 and CS^V, respectively. For the F^{III}20 concept using SS441 lowers the cost more than the CS^V due to high amount of steel in the concept. Using SS441 gives the same specific costs at a 55 % and 13 % lower power densities (for the two designs, respectively) as with Crofer. Assuming the power density value of the VPS/FCE stack and using SS441 estimates the costs to 390 €kWel^{-1} (goal B in Figure 7). A previous study found that Crofer22APU amounted to a higher cost of 1-14 % compared to SS441 [11]. The difference found here is 12 % for the light-weight design, assuming constant power density. Uncertainties of the theoretical SS441 scenario calculated herein should be mentioned. To our knowledge, long-term stack tests for SS441 IC with APS Cr-protection coating have not been performed. In a study [11] it is mentioned that the VPS/FCE concept uses SS441 and a PVD process for the coating material, the coating amount to around 30 % of the material costs, and also is the major bottleneck in their stack manufacturing. The DOE 2020 target is to reach 60,000 h of operation [22]. Long term stack testing in Jülich have shown that sudden effects and change in degradation behaviour can occur after more than 19,000 h of operation [27]. The longest running stack test found in literature was 9,000 h [45], thus, long term stability for SS441 based stacks are still to be proven.

5.4. Theoretical scenario replacing sequential sintering with co-sintering

A theoretical estimation of the effect on cost when replacing sequential sintering with co-sintering is performed. As previously reported for Jülich cells, the first three sequential sintering steps of anode substrate, anode and electrolyte can be replaced by one single co-sintering step, which lowers the number of sintering steps from 5 to 3 [30]. The calculations are performed at scenario for 25 MWy^{-1} production volume. It is estimated that this lowers the sintering and handling time from 76 to 45 h, which lowers the demanded kiln size. The energy consumption and personnel requirement is adapted accordingly with the lowered time. It is assumed that the material demands are not affected. Based on these analyses, the reduction in kiln size, thus investment, and not the reduction energy or personnel requirement, is dominant to cost-saving. Co-sintering is expected to give a certain reduction in the cell's power density as the microstructure can not freely be optimized for each layer [30]. However, previous reported values of co-sintered cell power density were tested in single cell measurements [30]. Transferring the cell performance to stack performance is complex as the cells were characterized in units with near ideal contacting and very low fuel utilization. In contrary to that, the cell performance cannot be kept in stack environment due to imperfect contacting and high fuel utilization. Thus a somewhat lower cell performance does not necessarily mean a lower stack

performance. But this has to be proven for the stack design individually. In order to compensate for possible power density reduction, more cell-layers will be needed in order to provide the required power. Since the stack Crofer parts are dominant in the their cost contribution, lower power density of the cells means a large addition to the cost due to the costly cell-periphery. When the steel parts become cheaper, the balance between cell costs, stack costs and cell performance shifts. Therefore, the cost analyses are done both on cell and stack level. In Figure 8, the estimated costs per kW on cell and stack level for co-sintered cells are shown. The horizontal lines represent the base-case with sequential sintered cells, the intersection between the curves and the base-case indicate at what level of power density reduction co-sintering becomes less cost efficient than sequential sintering. Comparing the cost of cells only A): For $F^{III}20$ at approx. 13 % power density reduction, and for CS^V at approx. 10 % power reduction co-sintering starts to be less cost effective. Comparing the cost at complete stack level B): at less than 5 % power density reduction co-sintering starts to be less cost effective for both concepts. For a cheaper stack support than the present, the break even points will be in between $\leq$5% and 13% and 10 % for $F^{III}2$ and CS^V, respectively.

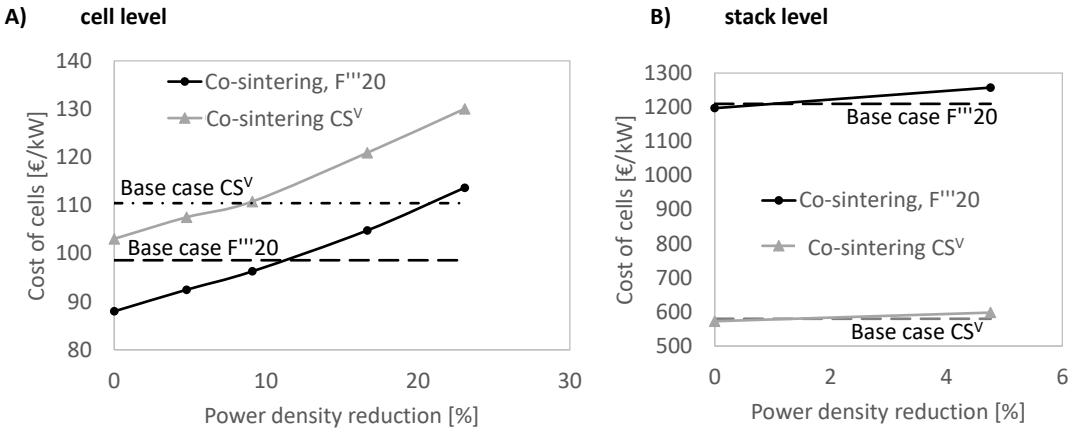

Figure 8: Theoretical calculation scenario for 25 MWy^{-1} applying co-sintering instead of sequential sintering, estimated direct manufacturing cost over cells area power density reduction (0 % corresponds to the area power density of base case) for A) cell level and B) stack level.

5.5. Comparison to previous studies

The direct manufacturing costs and fractions found in previous studies are given in Table 5. The total direct costs found for the Jülich designs are comparable, but higher than the previous studies. The sensitivity analysis (section 5.2) shows highest sensitivity to the material costs. The cost fractions for steel are lower in previous studies. It can thus be concluded that the difference in costs is mainly caused by this factor. Previous studies apply different types and lower amounts of steel (see section 3.2). Based on the stack building experience in Jülich, one important requirement in the mechanical design of the IC and frames is to provide sufficient bending- and torsional stiffness to ensure minimised cell bending, thus preventing short-circuiting of cells and defects causing gas leakage. Correct and evenly distributed contact pressure internally in each layer is also important. Thus, based on the stack building experience in Jülich, lowering the amount of steel is a technical challenge. The effect of altering the type of steel is discussed in section 5.3. The cost fraction contributed to labour is in similar range than previous studies at high scale production. But, most of the manufacturing cycle times in the previous studies are shorter than what is estimated achievable by the state-of-the-art ASC designs in Jülich. Even for non-continuous operations of short durations, they consistently assumed three working shifts [12, 11, 13], so that the requirements of machinery in these previous studies are lower.

6. Summary and conclusions

Based on the analyses herein, an evaluation of the manufacturing costs of two different Jülich anode supported SOFC stack designs is made. The direct costs of manufacturing the stack designs are estimated as: standard design: 2737 €kWel^{-1}-1210 €kWel^{-1}, and light-weight design: 2170 €kWel^{-1}-580 €kWel^{-1}, at the annual production volumes of 1-25 MWel, respectively. In comparison with previous comparable cost studies the estimated costs of the stacks are higher, but mainly in the same range. Material costs are estimated to be high compared to the other factors (at the 25 MWely^{-1} scale >65 %), which is in accordance with previous studies. However, main difference to previous studies is the relatively high cost of the metal support. The lower cost of the light-weight design investigated here compared to standard design (despite giving only 65% of its power density), is mainly due to the lower amount of steel. Minimizing steel costs is identified as one main important area of research and technical development to improve SOFC marketability. Jülich has shown that one way to reach this is by decreasing the amount of steel. Furthermore, a theoretical scenario applying low-cost stainless steel SS441 shows cost advantages over the base-case with Crofer steels. A theoretical scenario replacing sequential sintering with co-sintering shows limited cost-saving potential, on cell and especially on stack level. However, literature research concluded that although low-cost steels seems promising, long term stack tests (towards 60kh) are still lacking. It may be argued that the duration of stack testing for neither Crofer22H nor SS441 interconnects are sufficient to prove their long-term stabilities.

The sensitivity analyses show that the other main cost-sensitive factor is the stack power density. If the light-weight stack were to further improve the power density to the level of the standard design, the estimated cost decrease is 35 %. Based on a careful comparison of the designs, this is evaluated as feasible, and here contacting is identified as another main important technical challenge. Furthermore, the sensitivity analysis show that factors for contacting such as applying high-tech costly coating technique (e.g. APS), thicker Ni-mesh, increase in amount of spot-welding are not highly critical for the cost. As the cost of labour, energy and machinery is lower than materials, overall, more complex manufacturing techniques are worthwhile in the trade-off of material savings and improved power density. Nevertheless, simplification of the manufacturing and simplifying the design would be beneficial for the investment costs.

7. Outlook

The analysis presented herein indicates that optimization to obtain a minimum contact resistance between the stack contacting areas and material cost saving are key elements in achieving cost-efficient stack designs. It is shown that one way to achieve this is through high efficiency anode-supported SOFCs, in combination with a light-weight stack support. In the new generations of stack concept designs based on the CS^V design in Jülich particular attention has been given to the structural design, to develop concepts that ensure better utilisation of the cell performance with an optimised light-weight and material efficient design specialised for industrial-scale manufacturing. This study demonstrates that this approach is viable. The next generation stacks are pre starting or in the beginning of long-term performance and degradation tests. Furthermore, testing with low-cost stainless steel metal support/interconnects should be performed based on the knowledge drawn from this and previous studies.

8. Acknowledgements

The informations and advice applied from V. Bader, A. Cramer, D. Federmann F. Kurze, G. Mauer, R. Kauert, W. Herzhof, H.P. Buchkremer, P. Zapp, U. de Haart and S. M. Groß-Barsnick, A. Freund, K. Dahlhoff and all of colleagues at Forschungszentrum Jülich, and Mr. Schlemper from Fa. Proficut, Mr. J. Fr. Harboe and E. Ekeland are gratefully acknowledged.

References

[1] Q. Fang, L. Blum, P. Batfalsky, N. H. Menzler, U. Packbier, D. Stolten, Durability test and degradation behavior of a 2.5 kW SOFC stack with internal reforming of LNG, International Journal of Hydrogen Energy 38 (36) (2013) 16344–16353.

[2] W. L. Lundberg, S. E. Veyo, Conceptual design and performance analysis of a 300 MWe LNG-fueled pressurized SOFC/gas turbine power plant, ECS Proceedings Volumes 2001 (2001) 78–87.
[3] O. Costa-Nunes, R. J. Gorte, J. M. Vohs, Comparison of the performance of Cu–CeO2–YSZ and Ni–YSZ composite SOFC anodes with H2, CO, and syngas, Journal of power sources 141 (2) (2005) 241–249.
[4] C. O. Colpan, I. Dincer, F. Hamdullahpur, Thermodynamic modeling of direct internal reforming solid oxide fuel cells operating with syngas, International Journal of Hydrogen Energy 32 (7) (2007) 787–795.
[5] Energiforsk AB, Technology-review-SOFC, https://energiforskmedia.blob.core.windows.net/media/22411/technology-review-solid-oxide-fuel-cell-energiforskrapport-2017-359.pdf, accessed: 2018-07-25 (2017).
[6] S. J. McPhail, J. Kiviaho, B. Conti, The yellow pages of SOFC technology, international status of SOFC deployment 2017, IEA, http://www.enea.it/it/seguici/pubblicazioni/pdf-volumi/the-yellow-pages-of-sofc-technology-2017.pdf, accessed: 2019-01-02 (2017).
[7] L. Blum, L. B. De Haart, J. Malzbender, N. H. Menzler, J. Remmel, R. Steinberger-Wilckens, Recent results in Jülich solid oxide fuel cell technology development, Journal of Power Sources 241 (2013) 477–485.
[8] L. Blum, L. De Haart, J. Malzbender, N. Margaritis, N. H. Menzler, Anode-supported solid oxide fuel cell achieves 70 000 hours of continuous operation, Energy Technology 4 (8) (2016) 939–942.
[9] R. Rivera-Tinoco, K. Schoots, B. Van Der Zwaan, Learning curves for solid oxide fuel cells, Energy conversion and management 57 (2012) 86–96.
[10] J. H. J. S. Thijssen, The Impact of scale-up and production volume on SOFC stack cost, https://docplayer.net/19665792-The-impact-of-scale-up-and-production-volume-on-sofc-stack-cost-jan-h-j-s-thijssen-j-thijssen-llc-redmond-wa-usa.html, accessed: 2019-08-12 (2006).
[11] R. Scataglini, M. Wei, A. Mayyas, S. Chan, T. Lipman, M. Santarelli, A direct manufacturing cost model for solid-oxide fuel cell stacks, Fuel Cells 17 (6) (2017) 825–842.
[12] R. Scataglini, A. Mayyas, M. Wei, S. H. Chan, T. Lipman, D. Gosselin, A. D'Alessio, H. Breunig, W. Colella, B. James, A total cost of ownership model for solid oxide fuel cells in combined heat and power and power-only applications, Environmental Energy Technologies Division. Lawrence Berkeley National Laboratory.
[13] Battelle Memorial Institute, Manufacturing cost analysis of 1, 5, 10 and 25kW fuel cell systems for primary power and combined heat and power applications, https://www.energy.gov, accessed: 2018-10-01 (2017).
[14] M. R. Weimar, L. A. Chick, D. W. Gotthold, G. A. Whyatt, Cost study for manufacturing of solid oxide fuel cell power systems, Tech. rep., Pacific Northwest National Lab.(PNNL), Richland, WA (United States) (2013).
[15] B. D. James, A. B. Spisak, W. G. Colella, Manufacturing cost analysis of stationary fuel cell systems (2012).
[16] H. Ghezel-Ayagh, B. Borglum, Coal-Based SECA Program - FuelCell Energy Inc., 11th Annual SECA Workshop, Pittsburgh, PA, July 27-29, 2010 (2010).
[17] J. Otomo, J. Oishi, T. Mitsumori, H. Iwasaki, K. Yamada, Evaluation of cost reduction potential for 1 kW class SOFC stack production: Implications for SOFC technology scenario, International Journal of Hydrogen Energy 38 (33) (2013) 14337–14347.
[18] J. Otomo, J. Oishi, K. Miyazaki, S. Okamura, K. Yamada, Coupled analysis of performance and costs of segmented-in-series tubular solid oxide fuel cell for combined cycle system, International Journal of Hydrogen Energy 42 (30) (2017) 19190–19203.
[19] E. J. Carlson, Y. Yang, C. Fulton, Solid oxide fuel cell manufacturing cost model: Simulating relationships between performance, manufacturing, and cost of production, National Energy Technology Laboratory U.S. Department of Energy April 20, 2004, accessed: 2019-08-15 (2004).
[20] M. Ippommatsu, H. Sasaki, S. Otoshi, Evaluation of the cost performance of the sofc cell in the market, International Journal of Hydrogen Energy 21 (2) (1996) 129–135.
[21] A. M. Soydan, Ö. Yıldız, A. Durğun, O. Y. Akduman, A. Ata, Production, performance and cost analysis of anode-supported nio-ysz micro-tubular sofcs, International Journal of Hydrogen Energy 44 (57) (2019) 30339–30347.
[22] DOE technical targets for fuel cell systems for stationary (combined heat and power) applications, https://www.energy.gov/eere/fuelcells/doe-technical-targets-fuel-cell-systems-stationary-combined-heat-and-power, accessed: 2018-07-04 (2018).
[23] SECA fuel cell program moves two key projects into next phase, https://www.energy.gov/fe/articles/seca-fuel-cell-program-moves-two-key-projects-next-phase, accessed: 2019-08-06 (2009).
[24] R. A. George, N. F. Bessette, Reducing the manufacturing cost of tubular solid oxide fuel cell technology, Journal of power sources 71 (1-2) (1998) 131–137.
[25] F. J. Gardner, M. Day, N. Brandon, M. Pashley, M. Cassidy, Sofc technology development at rolls-royce, Journal of Power Sources 86 (1-2) (2000) 122–129.
[26] N. Margaritis, L. Blum, P. Batfalsky, D. Bohmann, S. Ceschini, Q. Fang, D. Federmann, J. Kroemer, R. Peters, R. Steinberger-Wilckens, Status of light weight cassette design of SOFC, ECS Transactions 68 (1) (2015) 209–220.
[27] L. Blum, U. Packbier, I. Vinke, L. De Haart, Long-term testing of SOFC stacks at Forschungszentrum Jülich, Fuel Cells 13 (4) (2013) 646–653.
[28] L. Blum, Q. Fang, L. de Haart, J. Malzbender, N. Margaritis, N. H. Menzler, R. Peters, Soc development at forschungszentrum jülich, ECS Transactions 78 (1) (2017) 1791–1804.
[29] N. H. Menzler, A. Beez, N. Grünwald, D. Sebold, Q. Fang, R. Vaßen, Diffusion-related sofc stack degradation, ECS Transactions 78 (1) (2017) 2223–2230.
[30] N. Menzler, J. Malzbender, P. Schoderböck, R. Kauert, H. Buchkremer, Sequential tape casting of anode-supported solid oxide fuel cells, Fuel Cells 14 (1) (2014) 96–106.
[31] S. M. Gross, T. Koppitz, J. Remmel, J.-B. Bouche, U. Reisgen, Joining properties of a composite glass-ceramic sealant,

Fuel Cells Bulletin 2006 (9) (2006) 12–15.
[32] W. J. Quadakkers, J. Pirón-Abellán, V. Shemet, Metallic materials in solid oxide fuel cells, Materials Research 7 (1) (2004) 203–208.
[33] L. Blum, P. Batfalsky, L. de Haart, J. Malzbender, N. Menzler, R. Peters, W. J. Quadakkers, J. Remmel, F. Tietz, D. Stolten, Overview on the Jülich SOFC development status, ECS transactions 57 (1) (2013) 23–33.
[34] J. Froitzheim, G. Meier, L. Niewolak, P. Ennis, H. Hattendorf, L. Singheiser, W. Quadakkers, Development of high strength ferritic steel for interconnect application in SOFCs, Journal of Power Sources 178 (1) (2008) 163–173.
[35] M. Bianco, J. Tallgren, J. Hong, S. Yang, O. Himanen, J. Mikkola, R. Steinberger-Wilckens, et al., Ex-situ experimental benchmarking of solid oxide fuel cell metal interconnects, Journal of Power Sources 437 (2019) 226900.
[36] X. Montero, F. Tietz, D. Stöver, M. Cassir, I. Villarreal, Comparative study of perovskites as cathode contact materials between an La0. 8Sr0. 2FeO3 cathode and a Crofer22APU interconnect in solid oxide fuel cells, Journal of Power Sources 188 (1) (2009) 148–155.
[37] N. Grünwald, D. Sebold, Y. J. Sohn, N. H. Menzler, R. Vaßen, Self-healing atmospheric plasma sprayed Mn1.0Co1.9Fe0.1O4 protective interconnector coatings for solid oxide fuel cells, Journal of Power Sources 363 (2017) 185–192.
[38] N. Menzler, P. Batfalsky, S. Groß, V. Shemet, F. Tietz, Post-test characterization of an SOFC short-stack after 17,000 hours of steady operation, ECS Transactions 35 (1) (2011) 195–206.
[39] N. Menzler, D. Sebold, O. Guillon, Post-test characterization of a solid oxide fuel cell stack operated for more than 30,000 hours: The cell, Journal of Power Sources 374 (2018) 69–76.
[40] N. Menzler, P. Batfalsky, A. Beez, L. Blum, S. Gross-Barsnick, L. Niewolak, Post-test analysis of a solid oxide fuel cell stack operated for 35,000 h, XII EFCF proceedings A11 (2016) 290.
[41] A. Materials, Stainless steel Grade 441 (UNS S44100), https://www.azom.com/article.aspx?ArticleID=8273, accessed: 2019-08-29 (2013).
[42] M. Bianco, M. Linder, Y. Larring, F. Greco, et al., Lifetime issues for solid oxide fuel cell interconnects, in: Solid Oxide Fuel Cell Lifetime and Reliability, Elsevier, 2017, pp. 121–144.
[43] C. Babelot, Q. Fang, L. Blum, G. Natour, Investigation of Ni-coated-steel-meshes as alternative anode contact material to nickel in an SOFC stack, International Journal of Hydrogen Energy.
[44] P. M. Editor Martin, Handbook of Deposition Technologies for Films and Coatings 3rd Edition Science, Applications and Technology, William Andrew, 2010.
[45] B. Borglum, E. Tang, M. Pastula, Development of solid oxide fuel cells at Versa Power Systems, ECS Transactions 35 (1) (2011) 63–69.
[46] Y. Chou, J. Stevenson, J. Choi, Long-term evaluation of solid oxide fuel cell candidate materials in a 3-cell generic stack test fixture, part III: Stability and microstructure of Ce-(Mn, Co)-spinel coating, AISI441 interconnect, alumina coating, cathode and anode, Journal of Power Sources 257 (2014) 444–453.
[47] R. Anghilante, D. Colomar, A. Brisse, M. Marrony, Bottom-up cost evaluation of SOEC systems in the range of 10–100 MW, International Journal of Hydrogen Energy 43 (45) (2018) 20309–20322.
[48] Statista, Industriestrompreise (inklusive Stromsteuer) in Deutschland, https://de.statista.com/statistik/daten/studie/252029/umfrage/industriestrompreise-inkl-stromsteuer-in-deutschland/, accessed: 2019-03-07 (2019).
[49] Argo, Free powerful Monte Carlo simulation, https://boozallen.github.io/argo/, accessed: 2019-08-12 (2019).